High temperature plasticity at twin boundary in Al: An in-situ TEM perspective

M. Larranaga, S. Lartigue-Korinek, Marc Legros, N. Combe, F. Mompiou

High temperature plasticity at twin boundary in Al: an in-situ TEM perspective

M. Larranaga[a], S. Lartigue-Korinek[b], M. Legros[a], N. Combe[a] and F. Mompiou[a]

[a] CEMES-CNRS and Université de Toulouse, 29 rue Marvig, 31055 Toulouse, France
[b] ICMPE, UMR 7182 CNRS-UPEC, 2-8 rue Henri Dunant, 94320 Thiais, France

ARTICLE INFO

Keywords:
in-situ TEM
dislocation
grain boundaries
plasticity
twin
disconnections

ABSTRACT

Coherent twin boundaries are of special importance in structural materials due to their strengthening ability by impeding dislocation motion while maintaining possible glide along their plane. Interactions of lattice dislocations with twin boundaries have been extensively studied experimentally and numerically but relaxation and deformation processes at high temperature are not fully understood. The reason is related to complex mechanisms of dislocation decompositions into disconnections, their further motion and possible reactions. Moreover, as in shear-coupled grain boundary (GB) mechanisms, motion of disconnections in the interface plane is expected to lead to twin motion perpendicular to its plane. Here, shear-coupled motion of a coherent twin in pure Al is explored during in situ straining in a transmission electron microscope (TEM) in a favorable geometrical configuration. Surprisingly, the twin boundary does not couple to shear but slightly migrates by propagating nanoscale incoherent facets. Although, disconnections of Burgers vector $1/6\langle 112\rangle$ have been extensively observed moving in the interface plane, their motion did not lead to migration as expected but presumably to GB sliding. This was interpreted by the motion of disconnections with opposite single and double steps in the [111] direction. Extensive dislocation/GB interactions were observed and reactions following absorption are interpreted by contrast analysis and motion observations. Incoming dislocations do not always decompose but often react with the GB disconnection microstructure which may lead to intergranular motions or dislocation emissions in the adjacent grain. As these processes usually involve disconnection climb in the interface plane, direct transmission, i. e. spatially and temporally correlated absorption/emission processes, is not observed as revealed by large scale observations. Finally, the internal disconnection microstructure of the twin boundary often forms networks which although flexible are found to slow down intergranular plasticity. Such networks should strongly control stress induced mechanisms in realistic GBs.

1. Introduction

Grain boundary (GB) strengthening is considered as an important factor for the development of structural materials. It is acknowledged since a long time that GBs play the role of obstacles to dislocations, but they can also constitute sources of strain accommodation by specific mechanisms such as transmission of slip through the GB, dislocation reflection, decomposition of dislocations into disconnections in the GB [19, 15]. In the recent years, mechanisms such as shear coupled migration, sliding and rotation, involving disconnections, i.e. dislocations with a step character [18], have received a peculiar attention [16, 40, 48, 39, 31]. Dislocation transmission or decomposition in the GB will depend on the disconnection mobility and their escape from the

*Corresponding author
mompiou@cemes.fr (F. Mompiou)
orcid(s):

impact location. All these mechanisms often require climb because they involve sessile disconnections [44, 47]. In the perspective of GB engineering, twin boundaries have always attracted a great attention especially in low energy stacking fault metals where they readily form. For example, nanotwinned copper is stronger due to grain refinement while maintaining a good ductility because of possible dislocation transfers and motions along twin planes [33, 51, 34].

Plastic mechanisms at twin interface in FCC metals involve both dislocation reactions and twin migration. The former was largely studied both experimentally by TEM [12, 53, 9, 30] and theoretically by atomistic modeling [23, 22, 3, 10, 13]. The latter mechanism can be described in terms of twinning dislocations, with a Burgers vector $1/6\langle 112\rangle$, moving along the twin boundary [26]. $1/6\langle 112\rangle$ vectors contained in the twin plane and $1/3\langle 111\rangle$ vectors normal to it are the basis vectors of the Displacement Symmetry Conserving (DSC) lattice and thus the smallest perfect Burgers vectors of the disconnections [25]. These disconnections will be called Shockley and Frank, respectively, by analogy with the partial dislocation in FCC lattice. Twin shear coupled migration can hence be viewed as a peculiar case of shear-coupled GB migration where the Shockley disconnection is a glissile disconnection of the $\Sigma 3$ DSC lattice along the (111) plane [2, 24]. Atomistic simulations were able to retrieve shear-coupling in $\Sigma 3$ bicrystalline copper [20]. This mechanism occurs by the thermal activation of an homogeneous disconnection loop nucleation in the twinning plane [57] similarly as what is observed in simulations of other GB shear coupled migration mechanisms [49].

At high temperature, plastic deformation mechanisms in twins are expected to be facilitated by easier dislocation decomposition, possible climb relaxation and easier Shockley disconnection nucleation leading to non-equilibrium GBs [43]. Although the evolution of intragranular disconnections during annealing has been studied experimentally in the past, in various metals and GBs, highlighting possible relaxation mechanisms [17, 46, 45], the influence of the stress on these processes at high temperature has been overlooked.

In this paper, we aim at contributing to the understanding of stress induced mechanisms occurring at a coherent $\Sigma 3$ GB at high temperature ($\approx 0.7\ T_m$) in pure Al. For this, we carried out in-situ TEM experiments on model bicrystals strained uniaxially in a geometrical condition maximizing the shear stress along the GB plane to favor shear coupled migration. The objective was also to investigate the role of dislocation-GB interaction i.e. possible absorption/emission or direct transmission mechanisms.

The paper is organized as follows. In a first part, we will describe the experiments and propose a methodology to interpret observations. Then, results of disconnection motions, and twin/dislocation interactions will be presented. Finally, we will discuss our interpretations in the light of literature.

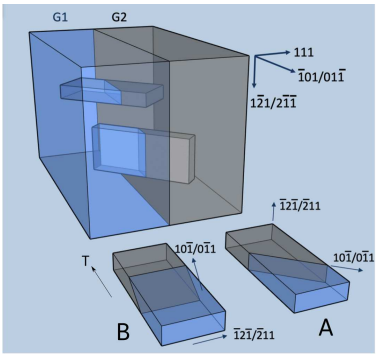

Figure 1: TEM samples extracted from a bulk bicrystal leading to straining configurations with a GB plane seen end-on in A and inclined in B. T refers to the straining axis.

2. Methodology and Experimental details

2.1. Sample preparation

An Al bi-crystal ($>$ 99.99 %) was grown by Bridgman method. Crystal orientation is derived by electron diffraction and the average disorientation is defined in angle/axis pair representation by 59.3° [0.59, 0.575, 0.568] [55]. The interface plane is normal to (111) without any facets in the TEM observation area. Hence the GB corresponds to a coherent $\Sigma 3$ twin boundary. 3 x 1 x 0.5 mm rectangular samples were then sliced from the bicrystal. The largest faces (3 x 1 mm) corresponding to the observation plane, were oriented in order to observe the GB plane in two different crystallographic configurations (Fig.1). In the first one (A, Fig.1), the GB plane is placed end on with respect to the observation plane and forms a 45° angle with respect to the long axis, i.e. the straining axis T. This configuration helps investigating possible steps on the GB when seen edge-on. In the second one (B, Fig.1), the GB plane normal is inclined about 45° with respect to the observation plane. In this configuration, the projection of the GB plane in the observation plane keeps a sufficient width while tilting around the straining axis, which facilitates the observation of disconnections under various diffraction conditions. In both configurations, the stress resolved in the GB plane is maximized in order to favor GB mechanisms, especially coupling and sliding. The block was then dipped into an aqueous solution of 50% HCl, 47% HNO_3 and 3% HF to optically reveal the GB. The marking of the GB position was preserved on at least one side of the sample surface throughout all the preparation procedures. Samples were then thinned down mechanically to 30 - 40 μm and finally electrochemically polished using a methanol solution with 33% nitric acid at T = -10°C.

2.2. Methodology

TEM observations were carried out in a JEOL 2010HC and JEOL 200EX microscopes. The acceleration voltage was usually decreased to 180 kV in order to minimize electron irradiation effects. Straining experiments were performed using a custom home made heating tensile holder operating in the range 300°C - 400°C. Observations were made during stress relaxation after strain increments. A special care was devoted to maintain the stress at a low level, limiting intragranular dislocation motion. Video sequences were recorded at 25 fps using a MEGAVIEW III camera and a mp4 encoding capture device. Crystal orientation, misorientation, planes/directions determination was derived from electron diffraction and conventional Bright Field/Dark Field (BF/DF) imaging, using pycotem [42]. When several imaging conditions are available, disconnection Burgers vectors can be determined by analyzing their contrast features [35]. When transient observations were made using hence a single diffraction condition, we used two beam simulations with the PCGBD program [21] in order to discriminate between different Burgers vectors. Owing to the nature of tensile deformation around small electropolished thin holes, we assume that in the observed area, local stress is parallel to the holder straining axis and thus that the resolved stress is maximum in the slip system with the highest Schmid factor [8]. Hence, we assume that observed intragranular dislocation glide is limited to systems with Schmid factor above 0.3. The nature of the slip planes can be easily inferred from the analysis of their traces and intersections with the GB plane [56]. Finally, using the fact that the contrast of disconnections depends on the Burgers vector direction (for a fixed line vector $\vec{u}$), the sense of their motion under stress can be compared to the direction of the Peach and Koehler force $\vec{F} = \bar{\bar{\sigma}}\vec{b} \times \vec{u}$. Although the above criteria are useful, they may not be discriminant enough. However, they allow to propose a limited number of scenarii. In the following, and for the sake of simplicity, details of the analysis will be omitted but could be found in the supplementary materials.

3. Results

3.1. Disconnection motion in the boundary

3.1.1. Nano-facets motion

Figure 2 shows intergranular activities in a sample strained in the end-on configuration (A in Fig. 1) at about 300 °C. When the GB is viewed end-on, here close to a ⟨112⟩ zone axis, nanometer high facets can be easily observed. Some of them noted h_i are shown under stress during a 52 s time interval (Fig. 2a-b). The step heights are of the order of 2-8 nm. Image difference (Fig. 2c) using the fiduciary markers X indicates a motion under stress of 52 nm of the facet h_4 while h_3 has remained immobile. Here and in the following figures, the straining axis is vertical. This motion indicates that nano-facets are sensitive to stress, hence

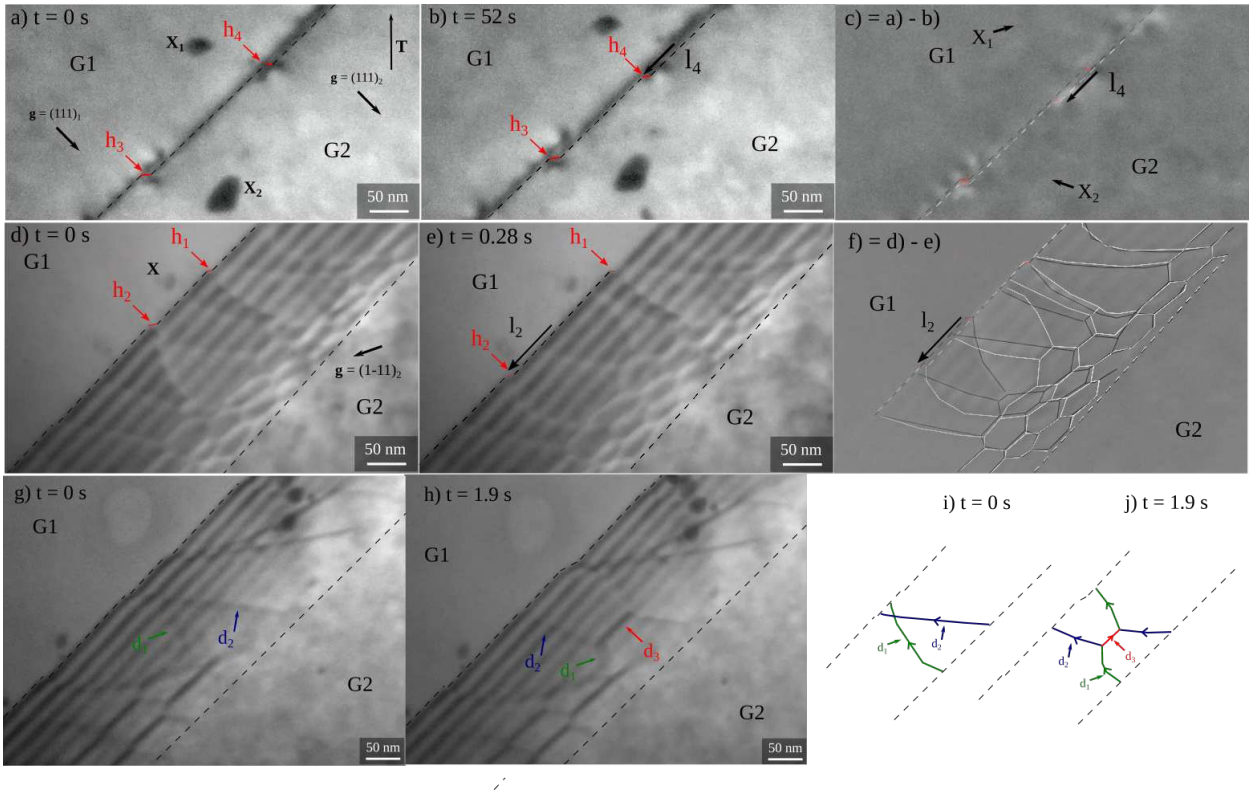

Figure 2: BF images from a straining experiment at 300 °C. a) - c) motion of nanometer high facets along the GB plane viewed end-on. The step h_4 has moved over a distance l_4 = 52 nm while the step h_3 remained immobile. d) - f) similar motions of steps h_1 and h_2 when the GB is viewed inclined. Note the presence of an hexagonal shape network. The rapid motion of h_2 is associated with complex network reorganization and disconnection crossing. g) - j) reaction between the disconnections d_1 and d_2, leading to the formation of a junction d_3. The GB is now inclined. This mechanism accredits the idea of network formation by disconnection motion within the GB.

contain disconnections. This is also indicated by the presence of localized bending contours along the GB plane in the vicinity of the steps. Although, nano-facets have moved, it is not possible owing to the scale of the observation to allow a measurement of a shear. Migration of {112} facets along coherent Σ 3 GB were observed by [37] and their height corresponds to a pure step, i.e. a three-layer normal to (111) (see also Fig. 4). Here, the existence of steps of several nanometers indicates that their motion should be at least composed of 10 pure steps. When viewed inclined about 25° with respect to the straining axis, the GB indeed shows several disconnections (Fig. 2d-e). At the sample surface, disconnections are connected to steps, here named h_1 and h_2. In the bottom part of the GB, a network can be observed. During straining, the motion of the two steps can also be tracked using image difference (Fig. 2f). It can be seen that h_2 moves abruptly of about 75 nm in 0.28 s, while h_1 remains immobile. These two observations showing a jerky motion tend to indicate that disconnections are pinned presumably due to their crossing. It can indeed be noted that a complex reorganization of the bottom network operated during step motion. Figure 2g-h is a clearer example

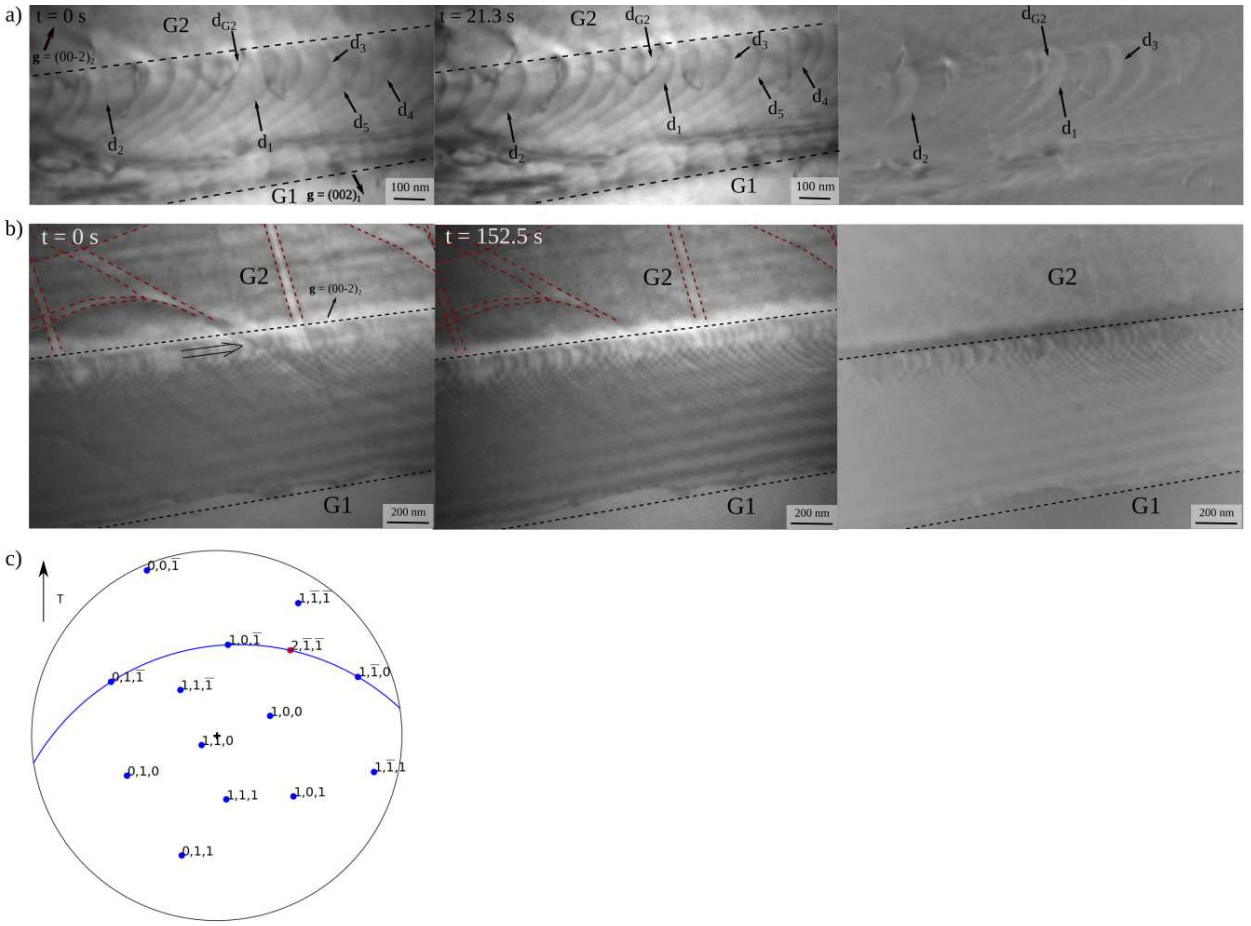

Figure 3: a) two pictures and their difference after the motion of curved disconnections d_i in an inclined GB. d_{G2} is an immobile disconnection. b) two pictures and their difference after motion of 76 disconnections over 152.5 s. Image difference is realized using dislocation traces in dotted lines as fixed markers in G2. c) stereographic projection of G1. In blue is shown the GB plane and in red the direction of the Burgers vectors in G1.

of interactions, where disconnections d_1 and d_2 initially crossing each other, eventually form a junction d_3 almost parallel to the GB trace. A corresponding sketch is shown in Fig. 2i-j. This observation supports the existence of a mechanism of disconnection interactions leading to stable networks as seen below in Fig. 6.

3.1.2. Sliding

Figure 3 reports observations at T = 350 °C in a GB inclined 45° with respect to the sample surface (B in Fig. 1). Crystal orientation in the G1 reference frame is shown in the stereographic projection (Fig. 3c), indicating also in blue the GB plane $(111)_{1,2}$. A train of disconnections labeled d_i moved under stress along the GB (Fig. 3a-b) as highlighted by image difference obtained after a 21.3 s time interval. Disconnection d_{G2} previously inserted in the GB remains immobile and serves as a fixed marker. Disconnection motion appears jerky, as shown previously, associated with jump length up to several tens of nm within a frame interval (40

ms). Their curvature in the opposite direction of their motion indicates that they react to the applied stress by developing a line tension stress. This stress can be estimated in first approximation by the formula $\tau = \mu b/R$, μ being the shear modulus in the GB plane, b the Burgers vector length and R the radius of curvature (corrected from perspective effects). Taking μ = 32 GPa, as in the bulk, $b = a_0/\sqrt{6}$ (see in the following), leads to τ in the range 35-40 MPa. This value is quite large compared to typical bulk values but can be for a large part accounted to the fact that disconnections move in a thin foil, and thus are confined between the two oxide surface layers [41]. Typical stress values in sub-micron grain sizes are also in agreement with the present estimation [4].

Disconnection analysis has been performed using 5 different imaging conditions in two beam conditions with diffraction vectors either in G1 or G2. Results are shown in the Supplementary materials and lead to a Burgers vector $\vec{b} = 1/6[2\bar{1}\bar{1}]_1 = 1/6[11\bar{2}]_2$, i.e. a Shockley disconnection. With respect to the straining axis T, this disconnection has the highest Schmid factor of 0.43 among the 3 Shockley contained in the GB plane, as shown in the stereographic projection of G1 in Fig. 3c. Moreover, the direction of disconnection motion is in agreement with the Peach and Koehler force direction.

The dichromatic pattern, projected along the $[\bar{1}10]_1/[\bar{1}01]_2$ direction, of the $\Sigma 3$ GB is shown in Fig. 4. In blue are marked the coincident positions forming the CSL lattice. Black (white) symbols correspond to lattice positions in G1 (G2), while circles and squares are positions shifted along the projection direction by $1/4[\bar{1}10]_1$. The 3 Shockley disconnections are indicated by the vectors $b^i_{1/1}$ according to the notation introduced in [1]. The two indices indicate that the signed step height normal to the GB plane, associated to the disconnection, is $1 \times h_0$ in both grains, $h_0 = a_0/\sqrt{3}$ being the minimum height. Note that a Shockley disconnection, with a double step height $b^i_{-2/-2}$ can also be defined. The Shockley disconnection identified in Fig. 3 corresponds here to $-b^B$. Note here that $b^A = 1/6[11\bar{2}]$ is normal to the z axis while $b^B = 1/6[\bar{2}11]$ and $b^C = 1/6[1\bar{2}1]$ are inclined $\pm 30°$ from it.

Disconnection motions were frequently observed all along the GB plane over a long period of time. Figure 3b shows two snapshots taken between an interval of 152.5 s in a thicker area. At least 76 disconnections were observed passing from the left to the right of the image. An image difference, using slip traces (red dotted lines) as fiduciary markers does not show measurable GB migration, neither a relative shear displacement of the grain as previously observed in shear coupled in-situ experiments [48, 38]. Indeed, as disconnections, with a non null step height, move in the GB they should provoke GB migration as well as a relative shear displacement between both grains. In order to understand this absence of shear and migration, we first estimate that, our measurement accuracy is about 2 pixels, corresponding to a minimum displacement of about 9 nm. The shear

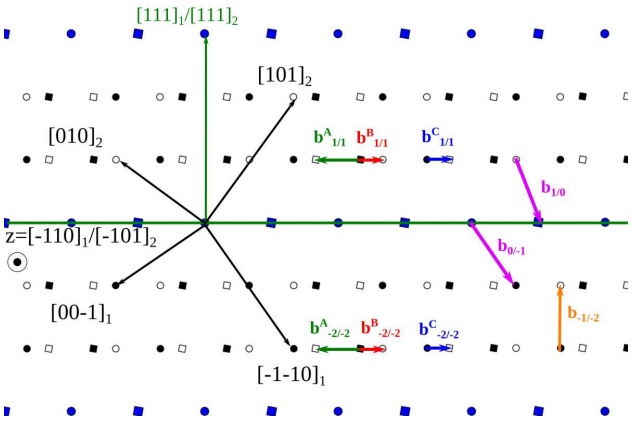

Figure 4: Dichromatic pattern of a Σ3 GB projected along the $[\bar{1}10]_1/[\bar{1}01]_2$ direction. Coincident positions are indicated in blue. White and black colors correspond to lattice positions in G1 and G2 respectively. The relative displacement between circle and square symbols is $1/4[\bar{1}10]_1$. Disconnections Burgers vectors are indicated as translations of the DSC lattice, i.e. translation linking black to white crystals. $b_{p/q}$ disconnections have p and q signed step heights expressed in both grains, respectively. In violet are shown 2 lattice dislocations.

produced by all the disconnections should be $s \approx 76\ a_0/\sqrt{6} \approx 12$ nm. As the Burgers vector direction make an angle of $\theta_1 = \angle(\vec{b}, \vec{b}_e) = 56.31°$ with respect to the electron beam ($\vec{b}_e$), the apparent shear in the observation plane should be of the order of $s_a = s\sin(\theta_1) = 0.83s \approx 10$ nm. This value is of the order of our detection threshold and thus could not be accurately determined. For a Shockley with a $h_0 = 0.234$ nm step height, the migration should be $m \approx 76h_0 = 17.8$ nm. As the angle between the electron beam and the GB plane normal $\theta_2 = \angle(\vec{n}, \vec{b}_e) = 38.3°$, the apparent expected migration should be $m_a = m/\sin\theta_2 = 1.61m \approx 28.7$ nm, which is definitely larger than our accuracy. As a consequence, the observation of a zero net GB migration by Shockley disconnections could be explained only if steps associated to the disconnection alternate in opposite directions. This can be achieved by considering the motion of both $b^B_{1/1}$ and $b^B_{-2/-2}$ Shockley disconnections as shown in Fig. 4.

3.2. Transmissions

Interactions between lattice dislocations and the GB is investigated in Figure 5. A bicrystal with an edge-on plane is strained at 400 °C. Stress level is here high enough to promote a more intense intragranular plastic deformation. About 15 events of dislocation absorption or emission were recorded. In Fig. 5a, an irregular low angle GB (LAGB) which trace is indicated by a dotted line is seen in the vicinity of the GB. It was formed by accumulation of edge dislocations gliding in G1. In the insert and in the corresponding snapshots taken at different times, the motion of two individual dislocations d_1 and d_2 moving toward the GB was monitored. During their motion they have left traces (TrS_1) at sample surface which are close to the expected trace of the slip plane $S_1 = (\bar{1}11)_1$ as shown in the stereographic projection (Fig. 5b). Dispersion in the position of

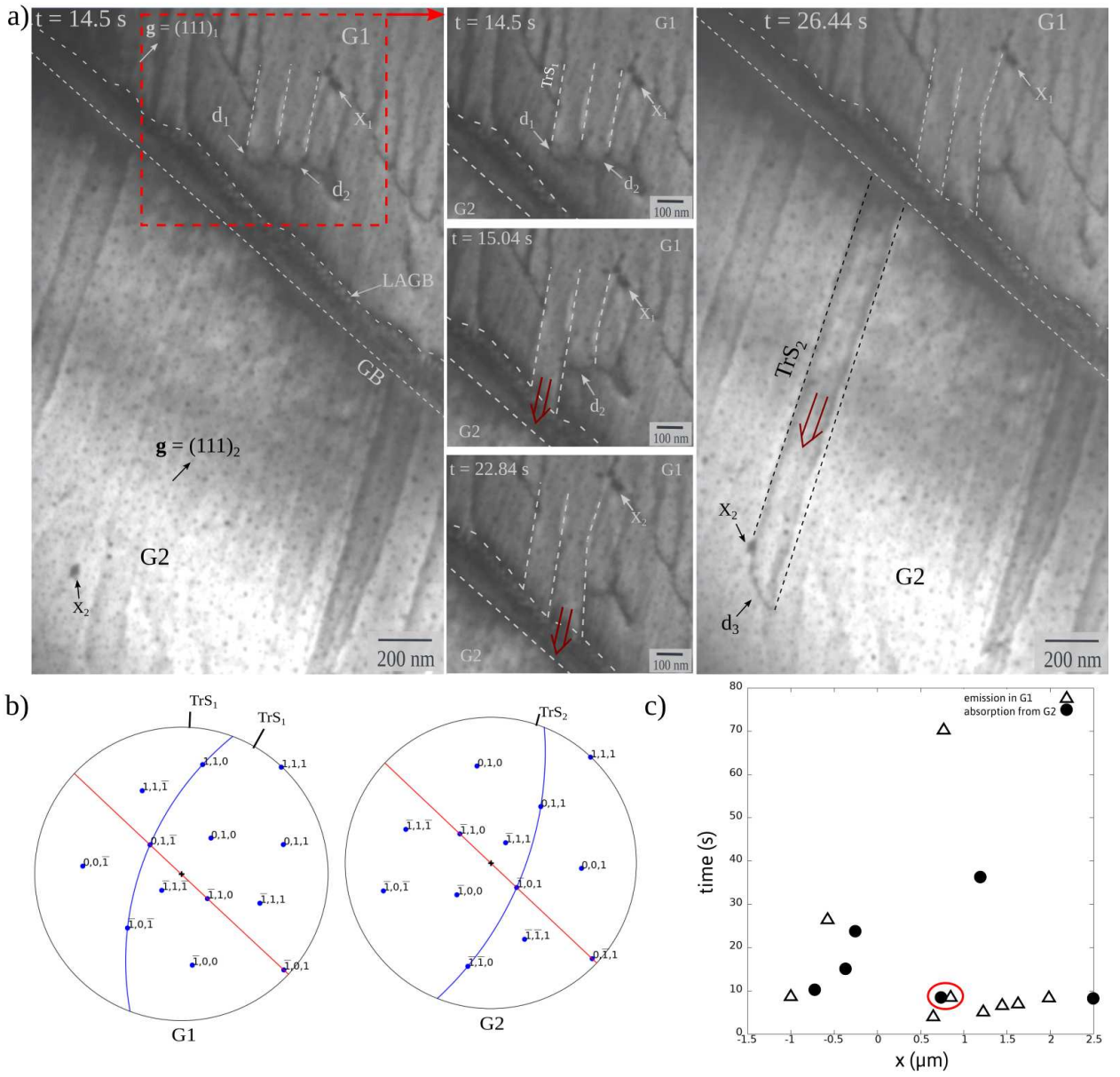

Figure 5: a) Insertion and emission of lattice dislocations in a GB. Details of insertion of dislocations d_1 and d_2 are shown in the insert and in 3 snapshots. After insertion, the emission of dislocation d_3 in grain G2 is reported. b) stereographic projections of the two grains. In red is the GB plane. Slip planes corresponding to the observed traces TrS_i are shown. c) A time/space plot of the insertion and emission events. The pair encircled in red corresponds to time correlated events.

TrS_1 corresponds to changes in plane of motion near the GB (t = 15.04 s). This changes may correspond to cross-slip or climb as previously observed in a Σ41 GB [48]. Dislocations were eventually absorbed in the GB at t = 22.84 s (Fig. 5a). At t = 26.44 s, dislocation d_3 is emitted from the GB and propagates in grain G2. Its slip trace (TrS_2) corresponds to the plane $S_2 = (\bar{1}1\bar{1})_2$ (Fig. 5b). Owing to the maximum Schmid factor criterion, d_1 and d_2 probably have a Burgers vector $b = 1/2[\bar{1}\bar{1}0]_1$ and $b = 1/2[\bar{1}\bar{1}0]_2$ for d_3 (Fig. 5b), corresponding

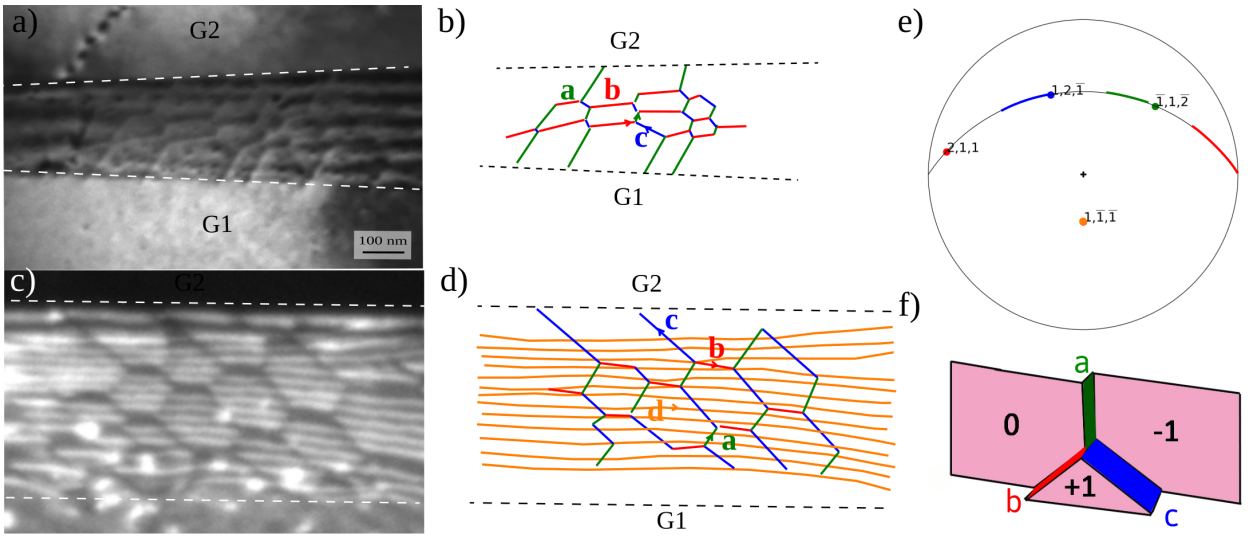

Figure 6: a) - c) Images of disconnection networks observed post-mortem after deformation. 4 disconnection types named *a* to *d* were analyzed. Their Burgers vectors and positions are indicated in b)-d) and their Burgers vectors (colored points) and line directions (colored segments) shown in the stereographic projection of G1 in e). f) is a 3D sketch of a network node showing a possible step arrangement. Relative signed positions of the GB plane are indicated in unit of $h_0 = a/\sqrt{3}$.

respectively to $b_{0/-1}$ and $b_{1/0}$ in Fig. 4. It should be noted that in this geometrical configuration, there are no common slip planes across the GB plane (in red in Fig. 5b). In order to get more insight in possible dislocation transmissions, we have reported in Fig. 5c, emission and absorption events in a time and space (position along the GB plane) plot. Spatial and temporal correlations can be searched along vertical and horizontal lines in this plot. Only a couple insertion/emission (encircled in red in Fig. 5c) shows a temporal correlation (at least at the frame rate acquisition time) but are weakly spatially correlated, the distance between them being of the order of 100 nm. Thus, no direct transmission could be inferred from our observations, but indirect transmission events occurring at a certain spatial scale could not be ruled out.

3.3. Disconnection network formation

A larger number of disconnection networks such as the one shown in Fig. 2 were observed. They present the same morphology with disconnections more or less spaced (see Supplementary materials for additional micrographs). As they are not distributed evenly along the plane, they are thought to have an extrinsic origin. They were analyzed after deformation in order to determine their nature. Figure 6 presents two images of networks (Fig. 6a,c) and corresponding sketches (Fig. 6b,e). Four types of disconnections, named *a* to *d* can be found. Their Burgers vectors were determined by observing their asymmetrical contrasts as shown in Fig. 3. *a*, *b* and *c* -type disconnections are the 3 Shockley disconnections. The directions of their lines are indicated

in Fig. 6e. They are spread in the GB plane, generally between 0° and 30° from their screw orientation. Disconnections of d-type are found to have $\vec{b} = 1/3[111]$ normal to the GB plane, i.e. Frank disconnections. Their Burgers vector $b_{\pm 1/\pm 2}$ is indicated in the dichromatic pattern (Fig. 4). In the network observed in Fig. 6c,d, their line direction is almost parallel to the GB trace, i. e. at the intersection of the GB with the sample surface. Contrary to Shockley dislocations, Frank dislocations should not be glissile in the GB plane. Fig. 6f shows a possible 3D configuration at a network node taking into account step heights for disconnection a, b, c. Numbers indicated the relative signed positions of the GB plane. Although the configuration could not be known from the present observations, this combination of single (a, b disconnections) and double (c disconnection) step heights will lead to network preserving average GB plane [28].

3.4. Detailed analysis of dislocation-GB interaction

Analyses of different interactions between incoming dislocations with the GB were studied in more details in order to get a better understanding of insertion and emission micromechanisms.

3.4.1. Reaction after dislocation insertion

Figure 7a presents an initial configuration, where a dislocation d_1 that has previously glided in G1, is inserted in the GB. The sequence described below occurred at the end of a relaxation period, i.e. when the stress level is close or below the elastic limit. The trace left (tr) is in agreement with slip in the $(11\bar{1})_1$ plane (see the stereographic projection for crystal orientation in Fig. 7c). Note that several other traces and several disconnections can be observed along the GB. Fig. 7a shows that d_1 is only partly inserted, the segment in the GB plane being oriented at the intersection of the glide plane and the GB plane, i.e. along the $\vec{u} = [\bar{1}10]_1$ direction. Considering that d_1 is the dislocation moving in $(11\bar{1})$ plane with the maximum Schmid factor, its Burgers vector should be along the [101] direction. As this dislocation moves in G1, from the bottom to the top of image, implies that the Burgers vector, with a line $\vec{u}$, is according to Peach and Koehler, $\vec{b}_1 = 1/2[101]_1$. In Fig. 8a, the image simulation of this dislocation under $\vec{g} = (002)_1$ shows a good agreement with the experimental image. It reproduces especially the GB fringe shift across the dislocation line. Thus, the inserted dislocation does not seem to decompose in the GB. As the Burgers vector has a component out of the GB plane, such decompositions should occur either by climb of two Shockley, i.e. $1/2[101]_1 = 1/6[112]_1 + 1/6[2\bar{1}1]_1$ or $1/2[101]_1 = 1/6[211]_1 + 1/6[1\bar{1}2]_1$ or a Frank and a Shockley $1/2[101]_1 = 1/6[121]_1 + 1/3[1\bar{1}1]$, or by the decomposition into a Frank and a glissile Shockley, i.e. $1/2[101]_1 = 1/6[1\bar{2}1]_1 + 1/3[111]_1$ [6, 27]. It is interesting to note that such decompositions did not occur at least in a sufficient time scale before the reaction occurs. Between t = 0 s and t= 1.5 s (Fig. 7b), the disconnection d_2 with a faint contrast, moved along the

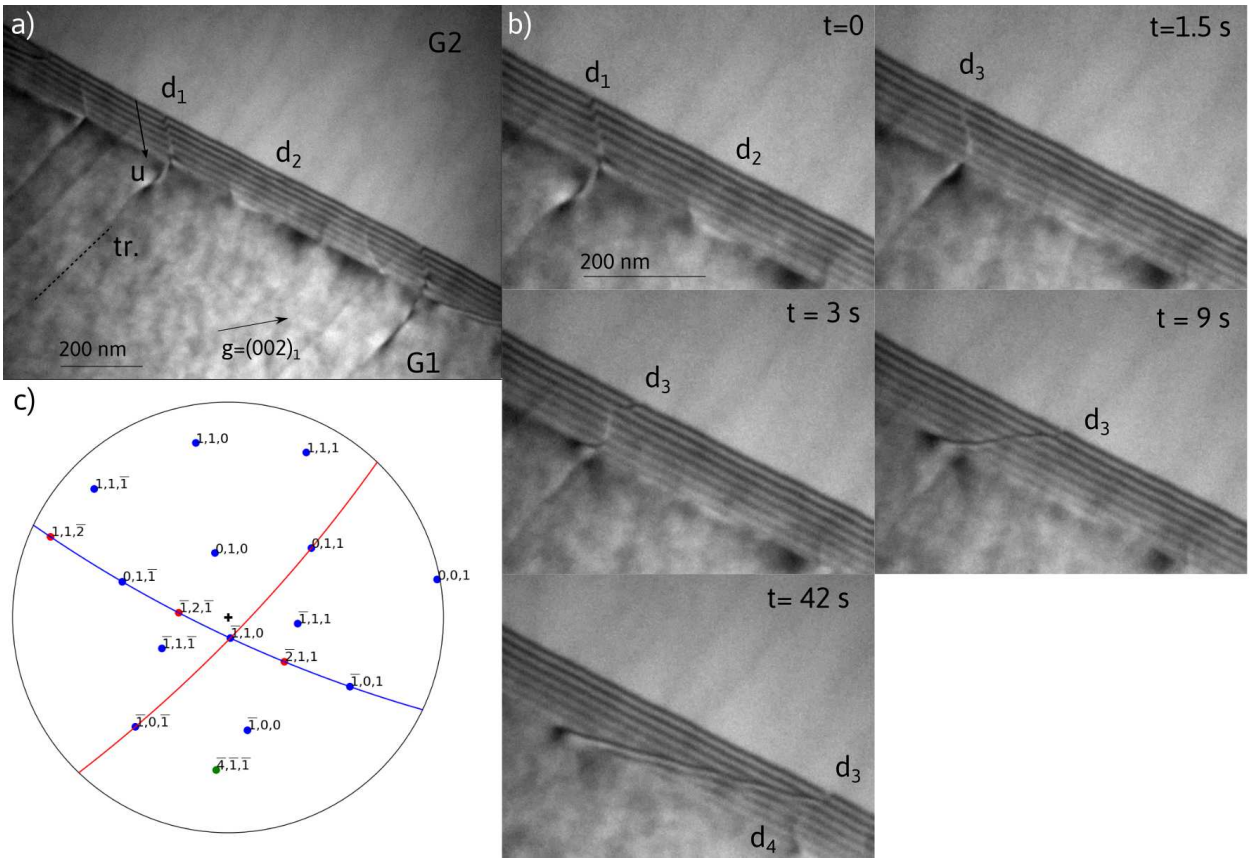

Figure 7: Reaction in the GB occurring after insertion of a lattice dislocation d_1 (a) with a moving disconnection d_2 leading to the formation of the d_3 disconnection (b). After reaction, the disconnection d_3 initially along the $[\bar{1}10]_1$ moved, rotated and eventually stopped along the $[01\bar{1}]_1$ direction presumably because of the disconnection d_4. c) stereographic projection of G1. In blue is indicated the GB plane and in red the incoming slip plane of d_1.

GB plane and eventually interacted with d_1. The disconnection motion appears very "hesitating" which indeed indicates that the stress level is here lower than in the previous observations such as in Fig. 3. The contrast of d_1 then changed indicating a change of the Burgers vector, i.e. a reaction leading to the dislocation d_3. After t=1.5 s, d_3 started to bend near the sample surfaces and eventually rotated until reaching a direction close to $[01\bar{1}]_1$ at t = 42 s (Fig. 7b). From then the disconnection became immobile. A total of 13 possible reactions, can be envisaged depending on the nature of d_3, either Shockley or Frank disconnections, or lattice dislocations (see Supplementary materials). Only two reactions lead to satisfactory contrasts but one of them lead to the formation of a $[100]_1$ disconnection which is thought to be energetically unfavorable owing to its large Burgers vector. Hence, the reaction should correspond to :

$$\vec{b}_1 + \vec{b}_2 = \vec{b}_3$$

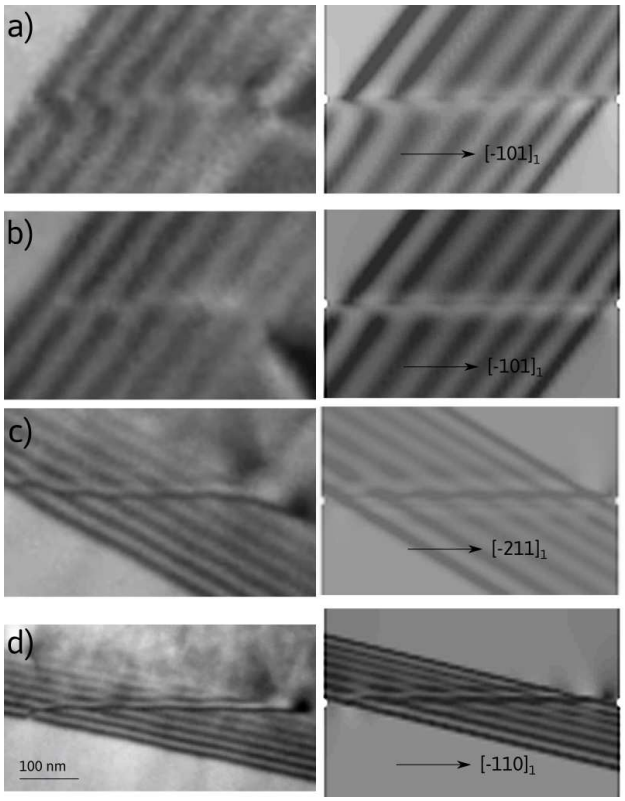

Figure 8: Contrast simulations (right) compared to experimental images (left) for the reaction shown in Fig. 7. a) d_1 with $\vec{b}_1 = 1/2[101]_1$ b)-d) d_3 with $\vec{b}_3 = 1/6[11\bar{2}]$. Line directions are indicated.

$$\frac{1}{2}[101]_1 + \frac{1}{6}[11\bar{2}]_1 = \frac{1}{6}[411]_1 = \frac{1}{2}[110]_2$$

Figures 8b-d show the agreement between the simulated contrasts of d_3 with different line directions as observed during its motion. In the dichromatic pattern (Fig. 4), it corresponds to the reaction $\vec{b}_{0/-1} + \vec{b}^{A}_{1/1} = \vec{b}_{1/0}$, which also highlights that the step height is conserved [6, 27]. According to the Peach and Koehler force, dislocation d_2 should move under stress in the opposite direction, i.e. away from d_1. However, a calculation of the elastic interacting stress (see Supplementary materials) indicates an attractive value of 2 MPa at a distance of 200 nm. This stress is supposed to be enough to trigger disconnection mobility as creep stress below 0.5 MPa is sufficient to activate shear coupled GB migration in Al at similar temperature [16]. At t = 3 s (Fig. 7b), the dislocation d_3 becomes fully inserted and starts to rotate and moves slowly and continuously along the GB. Owing the Burgers vector of d_3, this motion requires climb. The disconnection eventually finds an equilibrium position at t = 42 s (Fig. 7b) with a line direction close to $[01\bar{1}]_1/[\bar{1}10]_2$. From here the disconnection remains immobile. Considering that $\vec{b}_3 = 1/2[110]_2$, one would expect that it could escape in G2. However, d_3 line direction is not compatible with a slip plane in G2. The most probable slip plane is $(\bar{1}11)$, which intersects the

GB plane along $[0\bar{1}1]$. This line direction should have been reached with a further rotation of the disconnection. Although it is not clear why d_3 did not align along this direction, we can suspect that interaction with d_4 (Fig. 7b) prevents motion. It should be noted that at least three other disconnections with the same line orientation have been observed along the GB.

3.4.2. Reaction followed by dislocation emission

Figure 9 shows dislocation emission in grain $G1$ after reaction in the GB. Initially, a network of two arrays composed of straight disconnections, d_1 and d_2 can be observed (Fig. 9a). Disconnections are imaged here using $\vec{g} = (002)_1$. These two arrays do not seem to interact and form extended reaction junctions. At t = 0.02 s (Fig. 9b), a dislocation coming from grain G2, but invisible in the image, enters the GB. The insertion leads to the reinforcement of the contrast along d_1. A closer inspection indicates however that two disconnection lines can be distinguished close to the top surface, indicating that a reaction between the incoming dislocation and the d_1 disconnection occurs. Considering that the intersection line between the incoming dislocation and the GB is close to d_1 direction, i. e. $[01\bar{1}]_1$, indicates glide in the $(\bar{1}\bar{1}1)_2$ plane. The glide of the dislocation $\vec{b}_i = 1/2[0\bar{1}\bar{1}]_2$ leads to a maximum Schmid factor of 0.49. The direction of the Peach and Koehler force is compatible with slip from G2 toward G1. Although a similar analysis of the contrast cannot be rigorously carried out as previously, because the total elastic field of the disconnection networks cannot be easily taken into account in image simulation, a reasonable scenario can be proposed. The incoming dislocation $\vec{b}_i$ reacts first with $\vec{b}_1$, identified as a Shockley disconnection, leading to disconnection $\vec{b}_3$:

$$\vec{b}_i + \vec{b}_1 = \vec{b}_3$$

$$\frac{1}{2}[0\bar{1}\bar{1}]_2 + \frac{1}{6}[\bar{1}2\bar{1}]_2 = \frac{1}{6}[\bar{1}\bar{1}\bar{4}]_2 = \frac{1}{2}[0\bar{1}\bar{1}]_1$$

At t = 2.46 s, disconnections d_3 and d_2 start to repel at their intersection indicating a repulsive elastic interaction. No junction can be observed between the two disconnections. At that time, an embryo of dislocation d_4 can be observed. This embryo eventually expands at t = 3.14 s (fig. 9d) out of the GB plane, and finally d_4 escapes in G1 at t = 2.36 s (fig. 9e). The trace left at the sample surfaces (indicated by dashed lines in fig. 9e) is consistent with the $(11\bar{1})_1$ plane. The dislocation emission can be interpreted in the following way: dislocation d_3 is of the same type as dislocation d_2 which first explains the repulsion, i.e. $\vec{b}_3 = \vec{b}_2$. Dislocation emission hence corresponds to disconnection cross slip in G1, i.e. $\vec{b}_4 = \vec{b}_2$. Several spontaneous dislocation emissions have also been observed along the GB, but their detailed mechanisms could not have been revealed

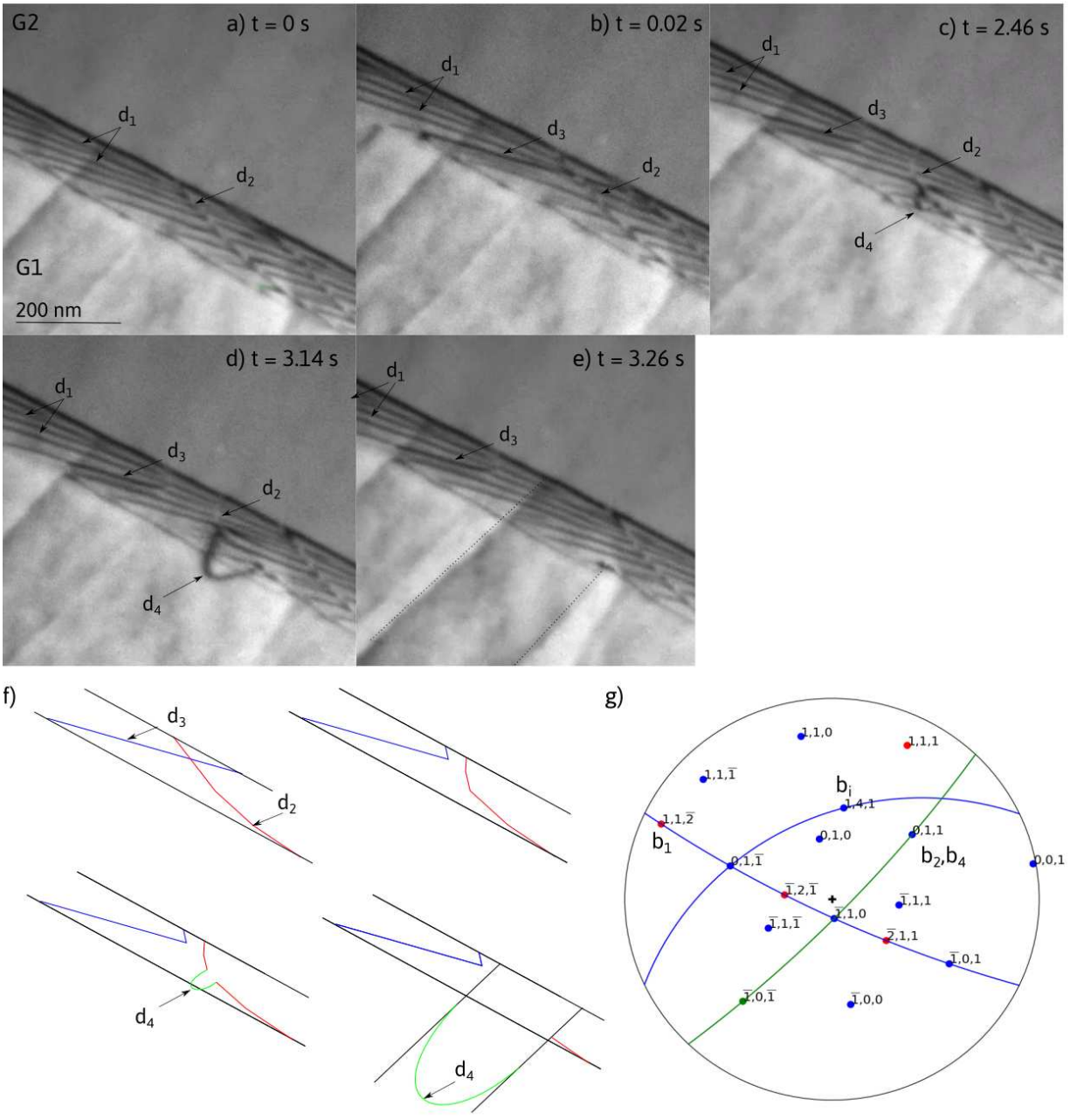

Figure 9: a) Area of the GB composed of two disconnection arrays (1 and 2). b) Reaction between a dislocation moving in G2 (invisible) with a disconnection d_1 forming a disconnection d_3. c) d_3 repulsively interacts with d_2. A cross-slip embryo forms in d_4 and eventually expands in d). Dislocation d_4 escapes and glides in G1. f) sketch of the reaction. g) stereographic projection of G1. Incoming G2 dislocation slip plane is indicated in blue and the d_4 slip plane in G1 in green.

due to the limited camera frame rate. Here the repulsion stress can be assumed to slow down the process by orienting d_2 away from the cross-slip direction, i.e. $[\bar{1}10]_1$. Emission eventually occurs by the formation of a cross slip embryo that spreads along the line (Fig. 9c-e) leading to an overall longer process. According

to the reaction above, the emitted dislocation has a Burgers vector $\vec{b}_4$=$\vec{b}_3$=$\vec{b}_2$=1/2$[0\bar{1}\bar{1}]_1$ and can glide in $(11\bar{1})_1$. Several points are consistent with this scenario: i) the contrast of isolated disconnections d_1 and d_2 is in qualitative agreement with the simulation in terms of intensity and asymmetry (shown in the Supplementary materials). ii) the two disconnection arrays are attractive but are not expected to form stable junctions as they would have an exotic Burgers vector $\vec{b}_1 + \vec{b}_2 = 1/6[\bar{2}1\bar{5}]_1$. iii) according to Peach and Koehler, the emitted dislocation moves away from the GB plane, in the $(11\bar{1})_1$ plane with a non negligible Schmid factor (0.35).

4. Discussion

4.1. Σ3 GB migration

At variance with other coincident GBs in Al, Σ3 GB boundary did not migrate significantly with stress at high temperature. A limited amount of migration was observed as a result of nanoscale facet motion that can be attributed to incoherent portion of the twin plane. Incoherent facets motion under electron beam has been analyzed in high resolution TEM [36, 37]. It is thought to occur by glide and climb of Frank 1/3[111] disconnection [36], or by a synchronized shear of three Shockley in three adjacent planes [37]. In the second interpretation, no shear strain is accommodated as the net Burgers vector of the Shockley is zero. The first interpretation would consist in the glide of Frank disconnection in the facet plane followed by their climb in the coherent interface, this latter motion requiring diffusion, which can be effective at the temperature where experiments were carried out. Such Frank disconnections have also been revealed at the coherent/incoherent junction in copper [51]. The hypothesis that incoherent facets become mobile under stress is thus consistent with a possible climb mechanism of Frank disconnections. Their motion is thus expected to produce a coupling factor only with a deformation component perpendicular to the coherent (111) plane, as also experimentally observed in a Σ41 GB [48].

Shear coupled GB migration is however expected as the result of motion of disconnections along the Σ3 GB plane. Motion of Shockley disconnections will lead to a large coupling factor of $\beta = 1/\sqrt{2} \approx 0.7$. Observation of Shockley and coupling factor measurement is in agreement with this conclusion both experimentally [26] in gold and in molecular simulations in copper [20]. In the present study, although a large number of moving Shockley has been observed, no migration was reported, suggesting that alternate disconnection steps in both grains should propagate. We suggest here that disconnection propagation would largely lead to sliding. Interestingly this work echoes molecular dynamic simulations investigating shear coupling in Σ3 GB showing that shear coupling is highly sensitive to shear stress direction. In particular, if the shear direction is along ⟨110⟩ direction, i.e. between the Burgers vector direction of Shockley disconnections, the coupling factor could be either reduced

to 0 or inverted. In a past article, we indeed have shown that alternative coupling modes could be activated when the shear stress is properly chosen [5, 7]. The present observation tends to indicate that in addition, modes carrying the same shear but with opposite migration directions can coexist, presumably because the probability rate to nucleate simple or double steps is similar at least at high temperature.

4.2. Interactions, reactions and transmission

Numerous evidence of interactions between dislocations and twin boundary have been recorded, but direct transmission was not observed. Criteria for slip transmission across GBs have been largely explored [32, 52, 29]. In [52], the parameter

$$M = \cos(\vec{l_i}, \vec{l_j}) \cos(\vec{b_i}, \vec{b_j})$$

, which takes into account the continuity of the Burgers vector and slip planes across the GB, should be maximum (i, j refers to the two grains, $\vec{l}$ to the intersection between the GB and the slip plane). The ideal situation will hence correspond to $M = 1$, for a screw dislocation cross-slipping between the two grains at the interface. Frequent dislocation transmission in front of dislocation pile-up [30] tends to indicate that the stress field generated in front of these pile-ups needs to be sufficient, in order to activate either the transmission or the reemission of dislocations in the adjacent grain. In general, the stress for transmission needs to be significantly larger than the yield stress [52]. An indirect transfer can also occur if GB sources are activated at a distance from the impact location along the GB plane. According to [29] transmission is expected to be favored if the magnitude of the Burgers vector of the residual disconnection left at the GB is small. Simulation works by [11, 10] indicate also that the associated step left should also be small. However, even in the most favorable case $M = 1$, the reaction may be complex and lead to decomposition as shown in different atomistic simulations [23, 11, 3]. Outcome of the reaction seems also strongly dependent on the ability of lattice dislocation to constrict (or not) before insertion [54, 50]. This situation should however been mitigated in Al where the stacking fault energy is large. Finally, the stress level for transmission is also strongly affected by the multiaxiality of the loading conditions [13].

The situation observed here is largely different. First, incoming dislocations usually have a mixed character. Second, observed interactions between dislocations and GB plane (Figs. 5, 7, 9) have shown that most probable slip systems, i.e. with a high Schmid factor, lead to $M = 0.41$ largely smaller than 1. However, thermal activation should favor transmission where climb is required, i.e. when the plane are discontinuous at the interface. Although climb process has been frequently observed, leading especially to line reorientation (Fig. 7), it appears to be insufficient to promote transmission, especially at low stress. Third, the absence of

pile-up prevents stress concentration. In such condition, absorption and reemission mechanisms are expected to occur in a more complex manner. From our observations, we indicate that intragranular reactions play a dominant role in these mechanisms. GB-dislocation interaction mechanisms often rely on the decomposition of lattice dislocation into disconnections, supported by many TEM observations [12, 14, 9]. Interestingly however here, we observe that dislocations may not decompose (Fig. 7) or probably remain stable in the GB (Fig. 9). This behavior in conjunction with the existence of Shockley disconnections is expected to provide additional mechanisms of intergranular plasticity, such as observed in Fig. 9. Finally, in very low stress condition, i.e. creep, dislocation transmission may be affected primarily by elastic interactions with disconnections in the GB plane, rather than disconnection decomposition and glide (Fig. 7).

4.3. Network formation

The complexity of possible decompositions and reactions is expected to lead to the formation of dislocation networks, shown in Fig. 6. They are composed of sets of Shockley and Frank disconnections which are the elementary DSC disconnections in $\Sigma 3$. These observations are coherent with reactions analyzed in a $\Sigma 3$ GB in pure Al [53]. No GB disconnection sources were observed during straining, which tends to indicate that networks mainly form by dislocation/GB interactions and further climb, glide and elastic interactions. Observation of disconnections moving along these networks indicates that they are flexible enough to be elastically overcome (Fig. 2). These intergranular reactions are thus expected to impede disconnection motion and hence lead to some hardening. This aspect has not been taken into account in plasticity but may be crucial in small grained materials as they can harden/suppress GB sliding or shear coupled GB migration mechanisms.

5. Conclusions

In-situ TEM straining experiments were carried out at high temperature on a $\Sigma 3$ coherent GB. The tensile geometry of the sample was designed to maximize the shear stress along the GB plane. Observations lead to the following conclusions:

- GB did not couple to shear. Only few nanometer high steps were observed moving along the GB plane under stress. Their large heights suggest that they are incoherent facets and that their motion should be associated to disconnections, supposedly Frank disconnections.

- Dislocation-GB interactions were reported. At a broader scale, dislocation transmission was prevented despite high temperature allowing climb motion. This absence of transmission is in agreement with unfavorable geometrical configuration. At a finer scale, analyses of dislocation absorption and emission,

reveal that mechanisms more complex than dislocation decompositions need to be considered to explain indirect transmission. These mechanisms occur at a significant time and length scale via disconnection reaction and glide or climb motion along the GB. This agrees with uncorrelated absorption and emission observations.

- Disconnection networks were frequently observed. They formed during plastic deformation by lattice dislocation incorporation/decomposition and interaction. They are composed by the 4 shortest DSC disconnections, i.e. 3 Shockley and a Frank disconnections. They impede disconnection motion but are sufficiently flexible to allow propagation of deformation along the GB plane.

Acknowledgements

This work receives the support of the ANR program RODIN (ANR-17-CE08-0007)

References

[1] Braisaz, T., Ruterana, P., Nouet, G., Pond, R.C., 1997. Investigation of {10 1 2} twins in Zn using high-resolution electron microscopy: Interfacial defects and interactions. Philosophical Magazine A 75, 1075–1095. doi:10.1080/01418619708214012.

[2] Caillard, D., Mompiou, F., Legros, M., 2009. Grain-boundary shear-migration coupling. II. Geometrical model for general boundaries. Acta Materialia 57, 2390–2402. doi:10.1016/j.actamat.2009.01.023.

[3] Chassagne, M., Legros, M., Rodney, D., 2011. Atomic-scale simulation of screw dislocation/coherent twin boundary interaction in Al, Au, Cu and Ni. Acta Materialia 59, 1456–1463. doi:10.1016/j.actamat.2010.11.007.

[4] Choi, H., Lee, S., Park, J., Bae, D., 2008. Tensile behavior of bulk nanocrystalline aluminum synthesized by hot extrusion of ball-milled powders. Scripta Materialia 59, 1123–1126. doi:10.1016/j.scriptamat.2008.07.030.

[5] Combe, N., Mompiou, F., Legros, M., 2016. Disconnections kinks and competing modes in shear-coupled grain boundary migration. Physical Review B 93, 024109. doi:10.1103/PhysRevB.93.024109.

[6] Combe, N., Mompiou, F., Legros, M., 2019. Heterogeneous disconnection nucleation mechanisms during grain boundary migration. Physical Review Materials 3, 060601. doi:10.1103/PhysRevMaterials.3.060601.

[7] Combe, N., Mompiou, F., Legros, M., 2021. Multiple coupling modes to relax shear strain during grain boundary migration. Acta Materialia 218, 117222. doi:10.1016/j.actamat.2021.117222.

[8] Coujou, A., Lours, Ph., Roy, N., Caillard, D., Clement, N., 1990. Determination of the local tensile axis direction in a tem in situ strained \gamma' single crystal—a finite element approach. Acta Metallurgica et Materialia 38, 825–837. doi:10.1016/0956-7151(90)90036-G.

[9] Couzinié, J., Décamps, B., Priester, L., 2005. Interaction of dissociated lattice dislocations with a \Sigma=3 grain boundary in copper. International Journal of Plasticity 21, 759–775. doi:10.1016/j.ijplas.2004.04.013.

[10] Dewald, M., Curtin, W.A., 2011. Multiscale modeling of dislocation/grain-boundary interactions: III. 60° dislocations impinging on Σ3, Σ9 and Σ11 tilt boundaries in Al. Modelling and Simulation in Materials Science and Engineering 19, 055002. doi:10.1088/0965-0393/19/5/055002.

[11] Dewald, M.P., Curtin, W.A., 2007. Multiscale modelling of dislocation/grain boundary interactions. II. Screw dislocations impinging on tilt boundaries in Al. Philosophical Magazine 87, 4615–4641. doi:10.1080/14786430701297590.

[12] Dingley, D., Pond, R., 1979. On the interaction of crystal dislocations with grain boundaries. Acta Metallurgica 27, 667–682. doi:10.1016/0001-6160(79)90018-X.

[13] Dupraz, M., Rao, S.I., Van Swygenhoven, H., 2019. Large scale 3-dimensional atomistic simulations of screw dislocations interacting with coherent twin boundaries in Al, Cu and Ni under uniaxial and multiaxial loading conditions. Acta Materialia 174, 16–28. doi:10.1016/j.actamat.2019.05.025.

[14] Elkajbaji, M., Thibault-Desseaux, J., 1988. Interactions of deformation-induced dislocations with \Sigma = 9(122) grain boundaries in Si studied by HREM. Philosophical Magazine A 58, 325–345. doi:10.1080/01418618808209929.

[15] George, A., 1988. Hardening mechanisms at grain boundaries: A microscopic approach. Revue de Physique Appliquée 23, 479–490. doi:10.1051/rphysap:01988002304047900.

[16] Gorkaya, T., Molodov, D.A., Gottstein, G., 2009. Stress-driven migration of symmetrical \langle 100 \rangle tilt grain boundaries in Al bicrystals. Acta Materialia 57, 5396–5405. doi:10.1016/j.actamat.2009.07.036.

[17] Grabski, M., Wyrzykowski, J., 1980. The effect of the spreading of grain boundary dislocations on the tensile behaviour of a fine-grained austenitic steel at high temperatures. Materials Science and Engineering 44, 229–237. doi:10.1016/0025-5416(80)90123-8.

[18] Hirth, J., Pond, R., 1996. Steps, dislocations and disconnections as interface defects relating to structure and phase transformations. Acta Materialia 44, 4749–4763. doi:10.1016/S1359-6454(96)00132-2.

[19] Hirth, J.P., 1972. The influence of grain boundaries on mechanical properties. Metallurgical Transactions 3, 3047–3067. doi:10.1007/BF02661312.

[20] Hu, Q., Li, L., Ghoniem, N., 2009. Stick–slip dynamics of coherent twin boundaries in copper. Acta Materialia 57, 4866–4873. doi:10.1016/j.actamat.2009.06.051.

[21] Humble, P., Forwood, C.T., 1975. Identification of grain boundary dislocations: I. The simultaneous two-beam method for obtaining experimental and computed electron micrographs. Philosophical Magazine 31, 1011–1023. doi:10.1080/00318087508226826.

[22] Jin, Z.H., Gumbsch, P., Albe, K., Ma, E., Lu, K., Gleiter, H., Hahn, H., 2008. Interactions between non-screw lattice dislocations and coherent twin boundaries in face-centered cubic metals. Acta Materialia 56, 1126–1135. doi:10.1016/j.actamat.2007.11.020.

[23] Jin, Z.H., Gumbsch, P., Ma, E., Albe, K., Lu, K., Hahn, H., Gleiter, H., 2006. The interaction mechanism of screw dislocations with coherent twin boundaries in different face-centred cubic metals. Scripta Materialia 54, 1163–1168. doi:10.1016/j.scriptamat.2005.11.072.

[24] Khater, H., Serra, A., Pond, R., Hirth, J., 2012. The disconnection mechanism of coupled migration and shear at grain boundaries. Acta Materialia 60, 2007–2020. doi:10.1016/j.actamat.2012.01.001.

[25] King, A.H., Smith, D.A., 1980. The effects on grain-boundary processes of the steps in the boundary plane associated with the cores of grain-boundary dislocations. Acta Crystallographica Section A 36, 335–343. doi:10.1107/S0567739480000782.

[26] Kizuka, T., 2007. Atomistic Process of Twin-Boundary Migration Induced by Shear Deformation in Gold. Japanese Journal of Applied Physics 46, 7396–7398. doi:10.1143/JJAP.46.7396.

[27] Larranaga, M., Mompiou, F., Legros, M., Combe, N., 2020. Role of sessile disconnection dipoles in shear-coupled grain

boundary migration. Physical Review Materials 4, 123606. doi:10.1103/PhysRevMaterials.4.123606.

[28] Larranaga, Melvyn, 2023. Mécanismes élémentaires de la migration de joints de grains couplée au cisaillement. Ph.D. thesis. Université Toulouse III. Toulouse.

[29] Lee, T., Robertson, I., Birnbaum, H., 1989. Anomalous slip in an FCC system. Ultramicroscopy 29, 212–216. doi:10.1016/0304-3991(89)90248-9.

[30] Lee, T.C., Robertson, I.M., Birnbaum, H.K., 1990. An In Situ transmission electron microscope deformation study of the slip transfer mechanisms in metals. Metallurgical Transactions A 21, 2437–2447. doi:10.1007/BF02646988.

[31] Liebig, J.P., Mačković, M., Spiecker, E., Göken, M., Merle, B., 2021. Grain boundary mediated plasticity: A blessing for the ductility of metallic thin films? Acta Materialia 215, 117079. doi:10.1016/j.actamat.2021.117079.

[32] Livingston, J., Chalmers, B., 1957. Multiple slip in bicrystal deformation. Acta Metallurgica 5, 322–327. doi:10.1016/0001-6160(57)90044-5.

[33] Lu, L., 2004. Ultrahigh Strength and High Electrical Conductivity in Copper. Science 304, 422–426. doi:10.1126/science.1092905.

[34] Lu, L., Zhu, T., Shen, Y., Dao, M., Lu, K., Suresh, S., 2009. Stress relaxation and the structure size-dependence of plastic deformation in nanotwinned copper. Acta Materialia 57, 5165–5173. doi:10.1016/j.actamat.2009.07.018.

[35] Marukawa, K., Matsubara, Y., 1979. A New Method of Burgers Vector Identification for Grain Boundary Dislocations from Electron Microscopic Images. Transactions of the Japan Institute of Metals 20, 560–568. doi:10.2320/matertrans1960.20.560.

[36] Medlin, D.L., Carter, C.B., Angelo, J.E., Mills, M.J., 1997. Climb and glide of $a/3\langle 111\rangle$ dislocations in an aluminium $\Sigma = 3$ boundary. Philosophical Magazine A 75, 733–747. doi:10.1080/01418619708207199.

[37] Medlin, D.L., Stobbs, W.M., Weinberg, J.D., Angelo, J.E., Daw, M.S., Mills, M.J., 1994. Migration dynamics of a $\Sigma3 {112}$ boundary in Aluminum. Mat. Res. Soc. Symp. Proc. 319, 6.

[38] Mompiou, F., Caillard, D., Legros, M., 2009. Grain boundary shear–migration coupling—I. In situ TEM straining experiments in Al polycrystals. Acta Materialia 57, 2198–2209. doi:10.1016/j.actamat.2009.01.014.

[39] Mompiou, F., Legros, M., 2015. Quantitative grain growth and rotation probed by in-situ TEM straining and orientation mapping in small grained Al thin films. Scripta Materialia 99, 5–8. doi:10.1016/j.scriptamat.2014.11.004.

[40] Mompiou, F., Legros, M., Boé, A., Coulombier, M., Raskin, J.P., Pardoen, T., 2013. Inter- and intragranular plasticity mechanisms in ultrafine-grained Al thin films: An in situ TEM study. Acta Materialia 61, 205–216. doi:10.1016/j.actamat.2012.09.051.

[41] Mompiou, F., Legros, M., Sedlmayr, A., Gianola, D.S., Caillard, D., Kraft, O., 2012. Source-based strengthening of sub-micrometer Al fibers. Acta Materialia 60, 977–983. doi:10.1016/j.actamat.2011.11.005.

[42] Mompiou, F., Xie, R.X., 2021. *Pycotem* : An open source toolbox for online crystal defect characterization from TEM imaging and diffraction. Journal of Microscopy 282, 84–97. doi:10.1111/jmi.12982.

[43] Nazarov, A., Romanov, A., Valiev, R., 1993. On the structure, stress fields and energy of nonequilibrium grain boundaries. Acta Metallurgica et Materialia 41, 1033–1040. doi:10.1016/0956-7151(93)90152-I.

[44] Pond, R.C., Smith, D.A., 1977. On the absorption of dislocations by grain boundaries. Philosophical Magazine 36, 353–366. doi:10.1080/14786437708244939.

[45] Poulat, S., Décamps, B., L. Priester, 1999. In-situ transmission electron microscopy study of the dislocation accommodation

in [101] tilt grain boundaries in nickel bicrystals. Philosophical Magazine A 79, 2655–2680. doi:10.1080/01418619908212016.

[46] Poulat, S., Décamps, B., Priester, L., 1998. Weak-beam transmission electron microscopy study of dislocation accommodation processes in nickel $\Sigma = 3$ grain boundaries. Philosophical Magazine A 77, 1381–1397. doi:10.1080/01418619808214259.

[47] Rajabzadeh, A., Legros, M., Combe, N., Mompiou, F., Molodov, D., 2013a. Evidence of grain boundary dislocation step motion associated to shear-coupled grain boundary migration. Philosophical Magazine 93, 1299–1316. doi:10.1080/14786435.2012.760760.

[48] Rajabzadeh, A., Mompiou, F., Lartigue-Korinek, S., Combe, N., Legros, M., Molodov, D., 2014. The role of disconnections in deformation-coupled grain boundary migration. Acta Materialia 77, 223–235. doi:10.1016/j.actamat.2014.05.062.

[49] Rajabzadeh, A., Mompiou, F., Legros, M., Combe, N., 2013b. Elementary Mechanisms of Shear-Coupled Grain Boundary Migration. Physical Review Letters 110, 265507. doi:10.1103/PhysRevLett.110.265507.

[50] Samaee, V., Dupraz, M., Pardoen, T., Van Swygenhoven, H., Schryvers, D., Idrissi, H., 2021. Deciphering the interactions between single arm dislocation sources and coherent twin boundary in nickel bi-crystal. Nature Communications 12, 962. doi:10.1038/s41467-021-21296-z.

[51] Sennour, M., Lartigue-Korinek, S., Champion, Y., Hÿtch, M.J., 2007. HRTEM study of defects in twin boundaries of ultra-fine grained copper. Philosophical Magazine 87, 1465–1486.

[52] Shen, Z., Wagoner, R., Clark, W., 1988. Dislocation and grain boundary interactions in metals. Acta Metallurgica 36, 3231–3242. doi:10.1016/0001-6160(88)90058-2.

[53] Solenthaler, C., 1990. On Dislocation Reactions in F.C.C. $\Sigma3$ Twin Boundaries. Materials Science and Engineering A 125, 57–70.

[54] Wang, Y.B., Sui, M.L., 2009. Atomic-scale *in situ* observation of lattice dislocations passing through twin boundaries. Applied Physics Letters 94, 021909. doi:10.1063/1.3072801.

[55] Wei, Y., Peng, Z., Kühbach, M., Breen, A., Legros, M., Larranaga, M., Mompiou, F., Gault, B., 2019. 3D nanostructural characterisation of grain boundaries in atom probe data utilising machine learning methods. PLOS ONE 14, e0225041. doi:10.1371/journal.pone.0225041.

[56] Xie, R.X., Larranaga, M., Mompiou, F., Combe, N., Zhang, W.Z., 2020. A general and robust analytical method for interface normal determination in TEM. Ultramicroscopy 215, 113009. doi:10.1016/j.ultramic.2020.113009.

[57] Zhou, H., Zhang, L., Qu, S., 2012. Temperature effect on critical shear stress for twin boundary migration. Computational Materials Science 60, 231–233. doi:10.1016/j.commatsci.2012.03.051.